

Preparation and microstructure of in-situ $(\text{ZrB}_2+\text{Al}_2\text{O}_3+\text{Al}_3\text{Zr})_p/\text{A356}$ composite synthesized by melt direct reaction

YANG Hua-jing, ZHAO Yu-tao, CHEN Gang, ZHANG Song-li, CHEN Deng-bin

School of Material Science and Engineering, Jiangsu University, Zhenjiang 212013, China

Received 23 March 2011; accepted 5 June 2011

Abstract: $(\text{ZrB}_2+\text{Al}_2\text{O}_3+\text{Al}_3\text{Zr})/\text{A356}$ composites were synthesized by melt direct reaction from $\text{A356}-(\text{K}_2\text{ZrF}_6+\text{KBF}_4+\text{Na}_2\text{B}_4\text{O}_7)$ system. The phase compositions and the microstructures of the as-prepared composites were investigated by XRD, SEM and TEM. The results show that the reinforcements are composed of ZrB_2 and Al_2O_3 ceramic phase particles and Al_3Zr intermetallic particles. The ZrB_2 particulates are easy to join together to form some particle clusters and distribute along the $\alpha(\text{Al})$ grain boundary. The morphologies of the ZrB_2 particulates are in hexagon-shape with the size of about 50 nm. The TEM investigation results of Al_3Zr indicate that Al_3Zr grows in the form of facet with the length-diameter ratio of about 20. The morphologies of Al_2O_3 particles are in rectangular-shape and ellipsoidal-shape, with the size of about 0.1 μm . In addition, the interfaces of the matrix and particles are net and no interfacial outgrowth is observed.

Key words: aluminum matrix composites; melt direct reaction; in situ particle; microstructure

1 Introduction

In situ aluminum matrix composites have received widespread attention in aerospace, automobile and electronic areas because of their good performances, such as high specific intensity and stiffness, excellent high temperature mechanical properties, good abrasion resistance and excellent near-net-shape production capacity [1–5]. Compared with the traditional ex situ composites, the in situ particulate reinforced aluminum matrix composites possess more advantages in microstructure, such as clean interfaces, strong interfacial bonding, fine particles and uniform distribution in matrix. Most of the previous reports are focused on single-phase particle reinforced aluminum matrix composites. For instance, LAKSHMI et al [6] developed TiB_2/Al matrix composite successfully in 1990's via the melt in-situ reaction, where the exothermic reaction occurred when two kinds of reactants (K_2TiF_6 and KBF_4) were added into the aluminum melt; HUANG et al [7] fabricated $\alpha\text{-Al}_2\text{O}_3/\text{Al}-\text{Cu}-\text{Si}$ alloy matrix composite by creating a substitution reaction from pure Al melt and CuO , SiO_2

powders. The single-phase particulate reinforced aluminum matrix composites have less variability in properties and applications than the multi-phase particulates reinforced aluminum matrix composites (MPRAMCs) because the type, the size and the distribution of the reinforcements of MPRAMCs can be mutual adjusted for the application requirements. So, the development and optimization of the MPRAMCs became a new subject [8–10]. But the reports on MPRAMCs are rare. Thus in this work, $(\text{ZrB}_2+\text{Al}_2\text{O}_3+\text{Al}_3\text{Zr})_p/\text{A356}$ MPRAMC composite were synthesized by melt in-situ reaction from $\text{A356}-(\text{K}_2\text{ZrF}_6+\text{KBF}_4+\text{Na}_2\text{B}_4\text{O}_7)$ system, and the microstructures were investigated.

2 Experimental

Raw materials were A356 alloy ingots (alloying component shown in Table 1) and three kinds of technical powders with 99.5% purity: potassium fluoborate (KBF_4), zirconium potassium fluoride (K_2ZrF_6) and sodium boricum ($\text{Na}_2\text{B}_4\text{O}_7 \cdot 10\text{H}_2\text{O}$). Firstly, potassium fluoborate, zirconium potassium fluoride, sodium boricum were pre-heated to dehydrate the

Foundation item: Project (50971066) supported by the National Natural Science Foundation of China; Project (20070299004) supported by Research Fund for the Doctoral Program of Higher Education of China; Project (2008-46) supported by Jiangsu Provincial '333' Project of training the High-level Talents Foundation, China; Project (BE2009127) supported by Jiangsu Provincial Science Supporting Item, China

Corresponding author: ZHAO Yu-tao; Tel: +86-15896380096, +86-13605288892; E-mail: zhaoyt@ujs.edu.cn

DOI: 10.1016/S1003-6326(11)61215-6

bonded water in an electric oven at 523 K for 3 h. Then the dried KBF_4 , K_2ZrF_6 and $\text{Na}_2\text{B}_4\text{O}_7$ powders were cooled, ground and screened. At the same time, A356 alloy ingots were molten in the electric furnace and held at 1123 K. Certain amount of dehydrated reactants powders were added with mechanical stirring assistance, the melt temperature was tested with thermal couple continuously. During the melt reaction process, the in situ reinforcements were formed in the molten A356 alloy. After 30 min, the melt was degassed and refined with the ZnCl_2 . When the melt temperature was 993 K, the melt was cast into a permanent mould.

The specimens (in the form of a block: 15 mm×15 mm×10 mm) were obtained from the as-prepared composite. The observed surface of the specimen was ground on emery paper from 180# to 1000# and polished. The XRD, SEM and TEM technologies were used to determine the phase component, microstructure and in situ particulate crystal morphology of the composite.

Table 1 Chemical composition of A356 alloy (mass fraction, %)

Si	Mg	Ti	Fe	Cu	Mn	Zn	Sn	Pb	Al
7.3	0.37	0.15	≤0.16	≤0.05	≤0.10	≤0.05	≤0.01	≤0.03	Bal.

3 Results and discussion

3.1 XRD analysis of prepared composite

In the experiment, sodium boron was used as a part of the reaction system due to that: 1) sodium boron can be taken as the source of boron during the composite process because the boron content of the $\text{Na}_2\text{B}_4\text{O}_7$ is 2.4 times as much as that of KBF_4 ; 2) sodium boron is a good flux for it can decrease the melting point of the reactants and accelerate the reaction.

Figure 1 shows the X-ray diffraction pattern of as-prepared composite from A356-($\text{K}_2\text{ZrF}_6+\text{KBF}_4+$

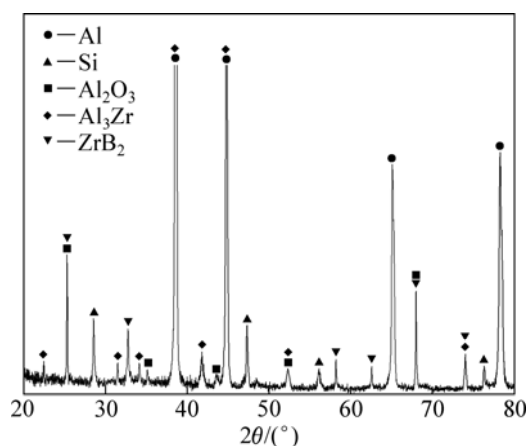


Fig. 1 XRD pattern of as-prepared composites from A356-($\text{K}_2\text{ZrF}_6+\text{KBF}_4+\text{Na}_2\text{B}_4\text{O}_7$) system

$\text{Na}_2\text{B}_4\text{O}_7$) reaction system. As shown in Fig. 1, the diffraction peaks of Al, Si, ZrB_2 , Al_3Zr and Al_2O_3 phases are observed, respectively.

To determine the progress of the reaction, the molten slag obtained after the reaction is also analyzed by XRD. It can be seen from Fig. 2 that the molten slag is mainly formed by K_2NaAlF_6 , KAlF_4 and K_3AlF_6 ; the presence of the Al_2O_3 may be due to the oxidation of matrix Al or the particulate sedimentation. The peaks unmarked are also the sedimentary ZrB_2 and Al_3Zr particles.

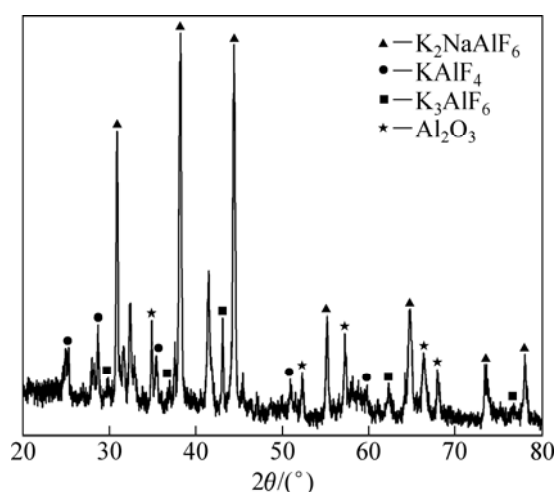
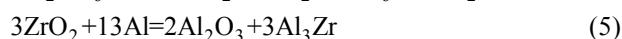
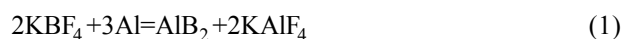


Fig. 2 XRD pattern of as-reaction finished oily substance on surface of melt

According to the above two XRD patterns and Refs. [11] and [12], the possible reaction occurring in the Al- $\text{Na}_2\text{B}_4\text{O}_7$ - K_2ZrF_6 - KBF_4 system can be illustrated as follows:



AlB_2 obtained from reactions (1) and (3) reacts with part of Al_3Zr which are formed in reactions (2) and (5):



Due to no AlB_2 found in Fig. 1, reaction (6) goes completely and ZrB_2 , Al_2O_3 and Al_3Zr particles are achieved finally in the composite.

The prepared composite melt could not be polluted by the oily K_2NaAlF_6 , KAlF_4 and K_3AlF_6 because they floated on the surface of composite melt and could be stripped off. In addition, those substances are good fluxes like the sodium boron, especially when the reactants were added in batches because they become the flux for the later reaction.

3.2 Microstructure of composite

Figure 3 shows the SEM images of the in-situ particle reinforcement composites with different theoretical volume fractions (ϕ_t): 5%, 10% and 15%. Due to the kinetic condition the in-situ reaction could not proceed sufficiently. So, the actual volume fractions of particulates are often less than the calculated theoretical values. Average recovery rate is 60%–80%, which is decreased with the increase of adding amount of reactants. It can be seen from Fig. 3, the particles are easy to join together to form some “particle clusters” and distribute along the $\alpha(\text{Al})$ grain boundary.

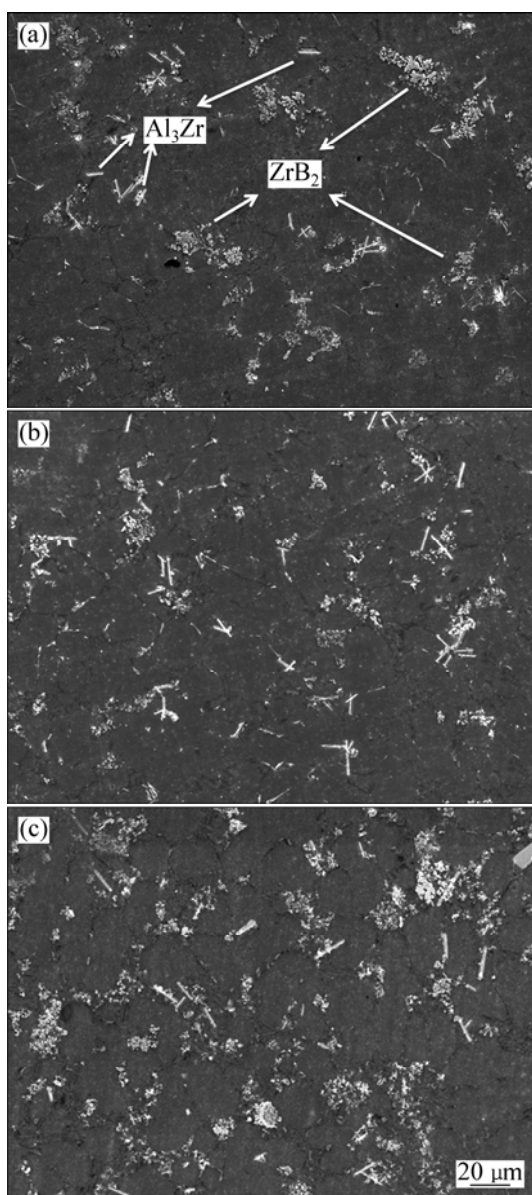


Fig. 3 SEM images of as-prepared composites with different theoretical volume fractions: (a) 5%; (b) 10%; (c) 15%

The high magnified SEM and TEM images and EDS patterns of the ZrB₂ particulate of (ZrB₂+Al₂O₃+Al₃Zr)/A356 composite are shown in Fig. 4. Figure 4(a)

shows the high magnification SEM image of ZrB₂ clusters and its EDS pattern. The morphologies of the ZrB₂ particulate are mainly hexagon-shaped and the size is about 50 nm, and the interfaces for the in-situ particulates and the aluminum matrix are not where no interfacial reactions are found. The calibration result of the diffraction ring indicates that the ZrB₂ is close-packed hexagonal structure and its lattice parameters are $a=b=3.169 \text{ \AA}$, $c=3.530 \text{ \AA}$.

Based on the Stokes particle floating rate formula, when the particle is small, it will move slowly and be captured by the growing matrix crystal grains to form a homogeneous and stable composite during the solidification [13]. The size of in-situ ZrB₂ particles is about 50 nm, so they would be captured by $\alpha(\text{Al})$ grains at usual setting rate and there would be less particles in the grain boundary. However, there is a great difference between the theoretical situation and the structure shown in Fig. 3 that most particles did not distribute in the $\alpha(\text{Al})$ grains while conglobated along the Al–Si grain boundary. It is considered that though the size of the in-situ ZrB₂ particles is quite small, but the interfacial energy of the aluminum melt is so high that the small particles reduce self-energy by getting together to form some “particulate clusters”. Moreover, the sedimentation of the particles in the melt becomes severe because of the increase of traveling speed of the clusters and the action of gravity. At the same time, during the solidification, the traveling speed of the clusters is superior to the solidification of the $\alpha(\text{Al})$ crystal grains, and then the particulate clusters are pushed to the front of solidification by the residual melt and eventually concentrate in the $\alpha(\text{Al})$ grain boundary.

Figure 5 shows TEM image and diffraction pattern of Al₃Zr reinforcements in (ZrB₂+Al₂O₃+Al₃Zr)/A356 composites. It can be found that the morphology of the Al₃Zr is rod like with the length-diameter ratio of 20. According to the crystal growth theory, the intermetallic compound grows in the form of facet. The atomic arrangement at the interface of liquid–solid is smooth. Thus single molecule is difficult to accumulate up on the smooth surface of the crystal and the growth of this interface will only depend on the stages occurring at the interface where the atoms diffused from the melt sedimentate [14,15]. The TEM results indicate that the facet is found on the surface of the Al₃Zr crystal which becomes the basis of Al₃Zr crystal growth. The result of the diffraction pattern shows that Al₃Zr crystal is tetragonal crystal and its lattice parameters are $a=b=4.009 \text{ \AA}$, $c=17.281 \text{ \AA}$.

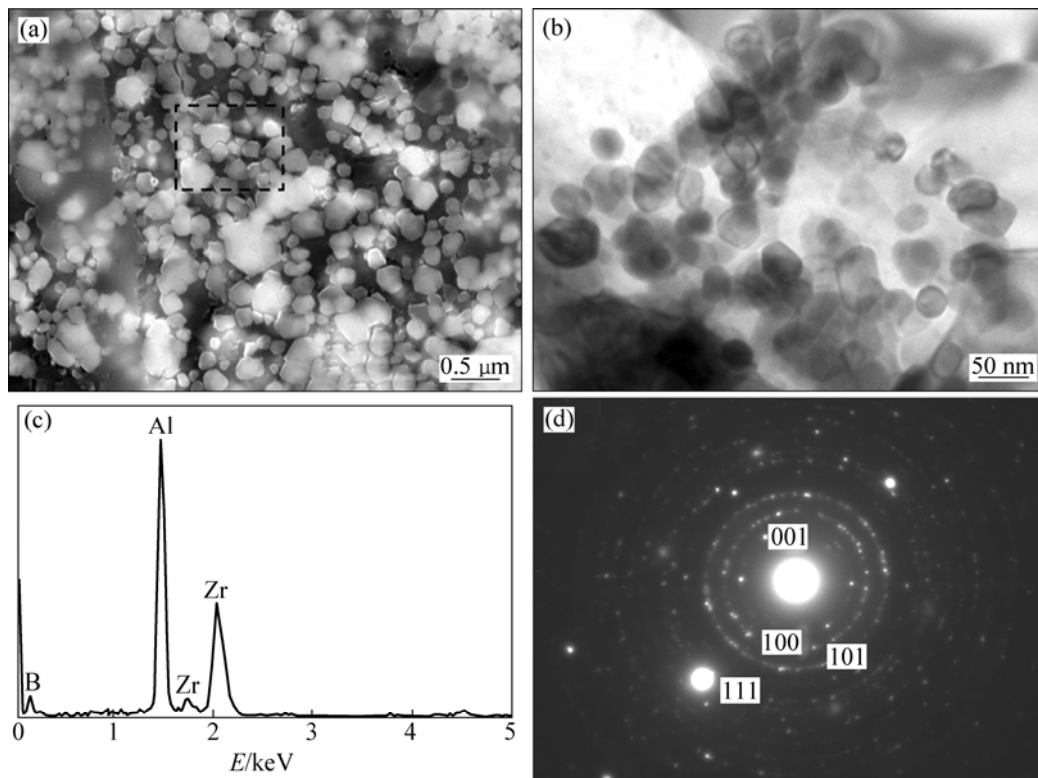


Fig. 4 SEM (a) and TEM (b) images, and EDS pattern (c, d) of ZrB_2 reinforcements in $(ZrB_2+Al_2O_3+Al_3Zr)/A356$ composites

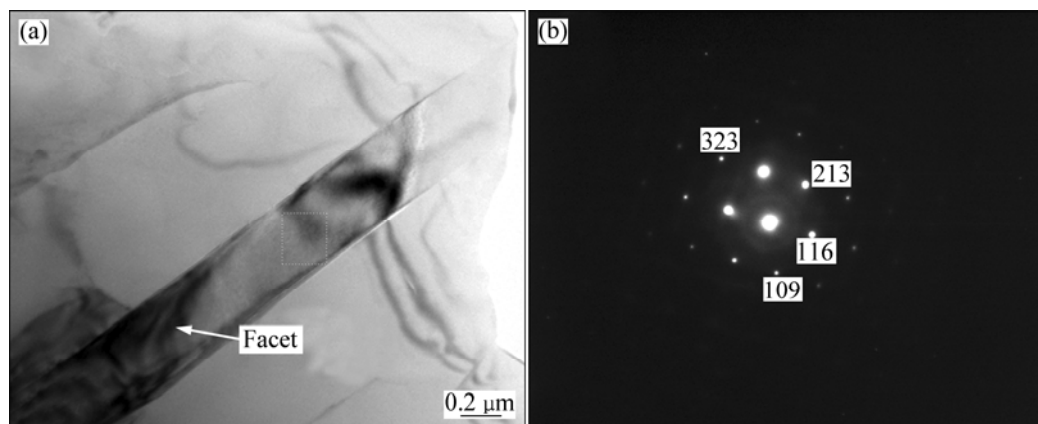


Fig. 5 TEM image (a) and EDS pattern (b) of Al_3Zr reinforcements in $(ZrB_2+Al_2O_3+Al_3Zr)/A356$ composites

Figure 6 shows the TEM and high resolution electron microscopy images of in situ Al_2O_3 ceramic reinforcements in $(ZrB_2+Al_2O_3+Al_3Zr)/A356$ composite. The size of Al_2O_3 particles is about $0.1 \mu m$ and the particles show two morphologies: rectangular and ellipsoidal which are showed as areas *B* and *C* in Fig. 6. The size of the particles with different morphology is about $0.1 \mu m$ and the particle/Al interfaces are smooth. The high resolution electron microscopy results show that Al_2O_3 particles with different morphologies both belong to the orthorhombic system and the lattice parameters are $a=7.934 \text{ \AA}$, $b=7.956 \text{ \AA}$, $c=11.711 \text{ \AA}$.

4 Conclusions

1) ZrB_2 , Al_2O_3 and Al_3Zr multi-phase particulates reinforced A356 matrix composites are fabricated from $A356-(KBF_4+K_2ZrF_6+Na_2B_4O_7)$ system by in-situ melts reaction technology.

2) The XRD results show that ZrB_2 , Al_2O_3 and Al_3Zr particles are contained in the as-prepared composite. The crystal structure of ZrB_2 is close-packed hexagonal with lattice parameters, $a=b=3.169 \text{ \AA}$, $c=3.530 \text{ \AA}$ and the micro morphologies of the ZrB_2

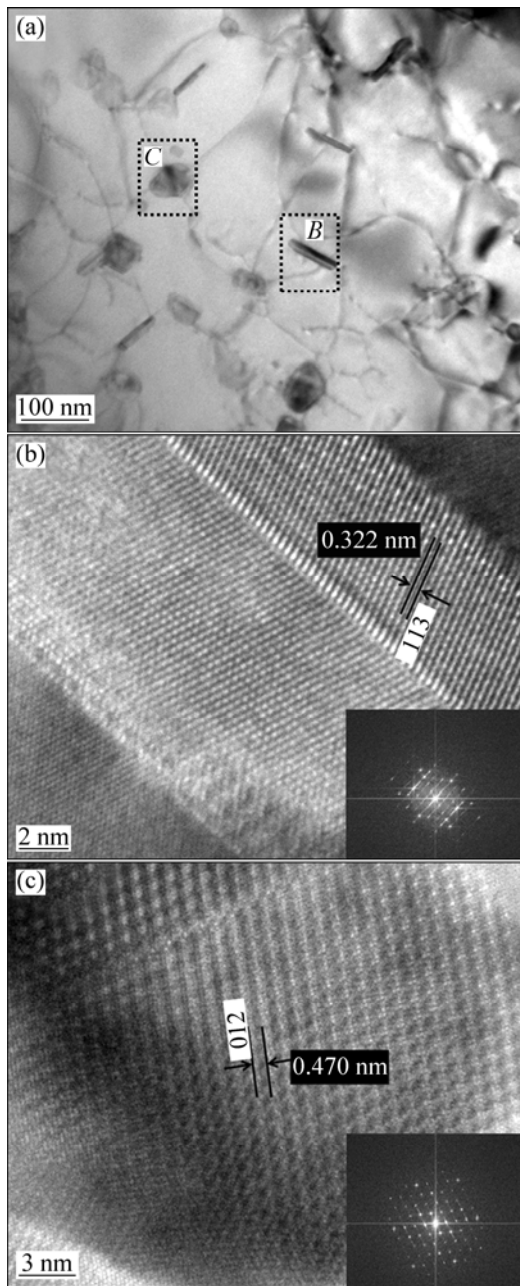


Fig. 6 SEM (a) and high resolution electron microscopy (b, c) images of Al_2O_3 reinforcements in $(\text{ZrB}_2+\text{Al}_2\text{O}_3+\text{Al}_3\text{Zr})/\text{A356}$ composites

particulate are mainly hexagon with the size of about 50 nm. The fine ZrB_2 particles are joined together to form some “particle clusters” and distribute along the $\alpha(\text{Al})$ grain boundary. Al_3Zr crystal is tetragonal with the lattice parameters, $a=b=4.009 \text{ \AA}$, $c=17.281 \text{ \AA}$. The morphology of Al_3Zr is rod-like with the length-diameter ratio of about 20. The morphologies of Al_2O_3 particles with size of $0.1 \mu\text{m}$ are rectangular and ellipsoidal, and crystals are orthorhombic with the lattice parameters, $a=7.934 \text{ \AA}$, $b=7.956 \text{ \AA}$, $c=11.711 \text{ \AA}$. The interfaces of the matrix and particles are net and no interfacial outgrowth is observed.

References

- [1] ZHU He-guo, MIN Jing, LI Jian-liang, AI Ying-lu, GE Liang-qi, WANG Heng-zhi. In situ fabrication of $(\alpha\text{-Al}_2\text{O}_3+\text{Al}_3\text{Zr})/\text{Al}$ composites in an Al-ZrO_2 system [J]. *Composites Science and Technology*, 2010, 70(15): 2183–2189.
- [2] TJIONG S C, MA Z Y. Microstructural and mechanical characteristics of in situ metal matrix composites [J]. *Materials Science and Engineering*, 2000, 29(3–4): 49–113.
- [3] KUMAR S, CHAKRABORYY M, SUBRAMANYA V, SARMA, MURTY B S. Tensile and wear behavior of in situ Al-7Si/TiB_2 particulate composites [J]. *Wear*, 2008, 265(1–2): 134–142.
- [4] WANG Hong-ming, LI Gui-rong, ZHAO Yu-tao, CHEN Gang. In situ fabrication and microstructure of Al_2O_3 particles reinforced aluminum matrix composites [J]. *Materials Science and Engineering A*, 2010, 527(12): 2881–2885.
- [5] LI G R, ZHAO Y T, WANG H M, CHEN G, DAI Q X, CHENG X N. Fabrication and properties of in situ $(\text{Al}_3\text{Zr}+\text{Al}_2\text{O}_3)_p/\text{A356}$ composites cast by permanent mould and squeeze casting [J]. *Journal of Alloys and Compounds*, 2009, 471(1–2): 530–535.
- [6] LAKSHMI S, LU L, GUPTA M. In situ preparation of TiB_2 reinforced Al based composites [J]. *Journal of Materials Processing Technology*, 1998, 73(1–3): 160–166.
- [7] HUANG Zan-jun, YANG Bin, CUI Hua, ZHANG Ji-shan. Study on the fabrication of Al matrix composites strengthened by combined in-situ alumina particle and in-situ alloying elements [J]. *Materials Science and Engineering A*, 2003, 351(1–2): 15–22.
- [8] TJIONG S C, WANG G S, GENG L, MAI Y W. Cyclic deformation behavior of in situ aluminum-matrix composites of the system $\text{Al-Al}_3\text{Ti-TiB}_2\text{-Al}_2\text{O}_3$ [J]. *Composites Science and Technology*, 2004, 64(13–14): 1971–1980.
- [9] ZHAO Yu-tao, ZHANG Song-li, CHEN Gang. $(\text{ZrB}_2+\text{Al}_2\text{O}_3+\text{Al}_3\text{Zr})_p/\text{Al-4Cu}$ composite synthesized by magneto-chemical melt reaction [J]. *Materials Science and Engineering A*, 2008, 487(1–2): 1–6.
- [10] LI G R, ZHAO Y T, DAI Q X, CHENG X N, WANG H M, CHEN G. Fabrication and properties of in situ synthesized particles reinforced aluminum matrix composites of Al-Zr-O-B system [J]. *Journal of Materials Science*, 2007, 42(14): 5442–5447.
- [11] YÜCEL B. Production of Al-Ti-B grain refining master alloys from $\text{Na}_2\text{B}_4\text{O}_7$ and K_2TiF_6 [J]. *Journal of Alloys and Compounds*, 2008, 458(1–2): 271–276.
- [12] FJELLSTEDT J, JARFORS A E W. On the precipitation of TiB_2 in aluminum melts from the reaction with KBF_4 and K_2TiF_6 [J]. *Materials Science and Engineering A*, 2005, 413–414: 527–532.
- [13] WANG Peng, MA Nai-heng, LI Xian-feng, WANG Hao-wei. The deposition of particulate in the in situ TiB_2 reinforced aluminum matrix composites [J]. *Special Casting & Nonferrous Alloys*, 2004, 9(2): 30–33. (in Chinese)
- [14] ZHAO Y T, CHENG X N, DAI Q X, CAI L, SUN G X. Crystal morphology and growth mechanism of reinforcements synthesized by direct melt reaction in the system Al-Zr-O [J]. *Materials Science and Engineering A*, 2003, 360(1–2): 315–318.
- [15] ZHAO Yu-tao, DAI Qi-xun, CHENG Xiao-nong, LIN Dong-yang, CAI Lan. Microstructure characterization of reinforcements in in-situ synthesized composites of Al-Zr-O system [J]. *Transactions of Nonferrous Metals Society of China*, 2005, 2(1): 108–112.

$(\text{ZrB}_2+\text{Al}_2\text{O}_3+\text{Al}_3\text{Zr})_p/\text{A356}$ 复合材料的 原位直接反应法制备及微观组织

杨华静, 赵玉涛, 张刚, 张松利, 陈登斌

江苏大学 材料科学与工程学院, 镇江 212013

摘要: 采用 A356-($\text{K}_2\text{ZrF}_6+\text{KBF}_4+\text{Na}_2\text{B}_4\text{O}_7$)作为熔体直接反应体系制备 $(\text{ZrB}_2+\text{Al}_2\text{O}_3+\text{Al}_3\text{Zr})/\text{A356}$ 复合材料。利用 XRD、SEM 和 TEM 等测试技术研究复合材料的相组成和微观组织。结果表明, 复合材料增强相由 ZrB_2 和 Al_2O_3 陶瓷相颗粒和 Al_3Zr 金属间化合物相颗粒组成。 ZrB_2 颗粒易团聚形成颗粒团簇并沿 $\alpha(\text{Al})$ 合金晶界分布; ZrB_2 颗粒的微观形貌为六边形, 尺寸在 50 nm 左右。TEM 研究发现, Al_3Zr 颗粒以小面形式生长, 其长径比约为 20; Al_2O_3 颗粒形貌为长方体状和椭圆状, 尺寸约为 0.1 μm 。此外, 基体与颗粒的相界面干净, 无界面反应物生成。
关键词: 铝基复合材料; 熔体直接反应; 原位颗粒; 微观组织

(Edited by YANG Hua)